TACC3 is a microtubule plus end–tracking protein that promotes axon elongation and also regulates microtubule plus end dynamics in multiple embryonic cell types

Belinda U. Nwagbara*, Anna E. Faris*, Elizabeth A. Bearce, Burcu Erdogan, Patrick T. Ebbert, Matthew F. Evans, Erin L. Rutherford, Tiffany B. Enzenbacher, and Laura Anne Lowery
Department of Biology, Boston College, Chestnut Hill, MA 02467

ABSTRACT **Microtubule plus end dynamics are regulated by a conserved family of proteins called plus end–tracking proteins (+TIPs). It is unclear how various +TIPs interact with each other and with plus ends to control microtubule behavior. The centrosome-associated protein TACC3, a member of the transforming acidic coiled-coil (TACC) domain family, has been implicated in regulating several aspects of microtubule dynamics. However, TACC3 has not been shown to function as a +TIP in vertebrates. Here we show that TACC3 promotes axon outgrowth and regulates microtubule dynamics by increasing microtubule plus end velocities in vivo. We also demonstrate that TACC3 acts as a +TIP in multiple embryonic cell types and that this requires the conserved C-terminal TACC domain. Using high-resolution live-imaging data on tagged +TIPs, we show that TACC3 localizes to the extreme microtubule plus end, where it lies distal to the microtubule polymerization marker EB1 and directly overlaps with the microtubule polymerase XMAP215. TACC3 also plays a role in regulating XMAP215 stability and localizing XMAP215 to microtubule plus ends. Taken together, our results implicate TACC3 as a +TIP that functions with XMAP215 to regulate microtubule plus end dynamics.**

Monitoring Editor
Paul Forscher
Yale University

Received: Jun 17, 2014
Revised: Jul 31, 2014
Accepted: Aug 26, 2014

INTRODUCTION

Microtubule (MT) plus end dynamics are regulated by a conserved family of proteins called plus end–tracking proteins (+TIPs; Akhmanova and Steinmetz, 2008). The regulation of MT plus end dynamics by +TIPs is critical to multiple aspects of embryonic development, including within the neuronal growth cone during axon outgrowth (Tanaka *et al.*, 1995; Lowery and Van Vactor, 2009). Despite their importance, few studies have examined how +TIPs affect MT dynamics in vertebrate growth cones (e.g., van der Vaart *et al.*, 2012; Lowery *et al.*, 2013; Marx *et al.*, 2013). In addition, it is unclear how the multitude of +TIPs interact with MTs and each other to control MT behaviors in these and other embryonic cell types.

The centrosome-associated protein TACC3, a member of the transforming acidic coiled-coil (TACC) domain family, is strongly implicated in regulating MT stability during mitosis (Gergely *et al.*, 2000a; Peset and Vernos, 2008). TACC3 was first identified as a MT-binding protein after immunostaining demonstrated its colocalization with MTs on centrosomes and mitotic spindles (Groisman *et al.*, 2000). Reports have shown that reducing the level of TACC3 leads to shorter astral and spindle MTs in worms (Bellanger and Gonczy, 2003; Le Bot *et al.*, 2003; Srayko *et al.*, 2003), flies (Gergely *et al.*, 2000b), and vertebrate cells (Kinoshita *et al.*, 2005; O'Brien *et al.*, 2005; Peset *et al.*, 2005), whereas overexpressing TACC3 leads to longer spindle MTs (Gergely *et al.*, 2000a; Peset *et al.*, 2005). As a result of these studies, TACC3 has been called a MT growth-promoting or stabilizing factor, at least in the context of MTs during mitosis (Gergely *et al.*, 2000a; Peset and Vernos, 2008).

This article was published online ahead of print in MBoC in Press (http://www.molbiolcell.org/cgi/doi/10.1091/mbc.E14-06-1121) on September 3, 2014.

*These authors contributed equally.

Address correspondence to: Laura Anne Lowery (Laura.lowery@bc.edu).

Abbreviations used: EB1, end-binding protein 1; GFP, green fluorescent protein; KD, knockdown; MO, antisense morpholino oligonucleotide; MT, microtubule; OE, overexpression; TACC, transforming acidic coiled-coil domain; +TIP, plus end–tracking protein.

© 2014 Nwagbara, Faris, *et al.* This article is distributed by The American Society for Cell Biology under license from the author(s). Two months after publication it is available to the public under an Attribution–Noncommercial–Share Alike 3.0 Unported Creative Commons License (http://creativecommons.org/licenses/by-nc-sa/3.0).
"ASCB®," "The American Society for Cell Biology®," and "Molecular Biology of the Cell®" are registered trademarks of The American Society for Cell Biology.

An unanswered question in the TACC3 field is how a protein that is primarily localized to the centrosome can have such a strong effect on MT length. It has been suggested that a primary function of TACC3 is to recruit the microtubule polymerase XMAP215 to the centrosome (Peset and Vernos, 2008). The interaction between TACC3 and XMAP215 has been well documented in multiple systems (Lee *et al.*, 2001; Kinoshita *et al.*, 2005; O'Brien *et al.*, 2005; Peset *et al.*, 2005), where it is apparent that TACC3 localizes XMAP215 to the centrosome and that normal mitotic spindle assembly requires their interaction. However, despite the well-known localization of XMAP215 at growing MT plus ends (Brouhard *et al.*, 2008), it has been unclear whether vertebrate TACC3 interacts with XMAP215 specifically at plus ends during interphase.

There has been some evidence that, in other systems, TACC proteins may bind to and regulate the plus ends of MTs (Peset and Vernos, 2008). Whereas the single TACC orthologue in *Drosophila* (called D-TACC) is highly concentrated at centrosomes in vivo (Gergely *et al.*, 2000b), green fluorescent protein (GFP)–tagged D-TACC was also observable as small puncta that emanate from the centrosome, likely corresponding to growing MT plus ends (Lee *et al.*, 2001). Furthermore, knockdown of D-TACC results in reductions in MT growth parameters in cultured fly cells, and *d-tacc* genetically interacts with the +TIP *CLASP* during the development of normal fly eye morphology (Long *et al.*, 2013). However, time-lapse imaging of fluorescently tagged TACC3 has not yet been examined in any vertebrate context, which would be necessary to determine whether TACC3 does, indeed, track MT plus ends. In addition, the mechanism by which vertebrate TACC3 regulates MT plus end dynamics is not known.

In addition to a general cellular role in the regulation of MT dynamics, there are also indications that TACC3 may play a specific role during neuronal development. TACC3 up-regulation occurs when PC12 cells are in the process of differentiating into neurons (Sadek *et al.*, 2003), and TACC3 is also involved in the maintenance of the neural progenitor pool during neocortical development (Xie *et al.*, 2007; Yang *et al.*, 2012). Moreover, *Xenopus* TACC3 expression is enriched in the developing embryonic nervous system (Tessmar *et al.*, 2002). However, a definite role for TACC3 within the embryonic neuronal growth cone during axonal outgrowth has not yet been elucidated.

In this article, we begin to investigate the potential function of TACC3 within the vertebrate developing nervous system by analyzing axon outgrowth parameters of cultured embryonic *Xenopus laevis* neurons after TACC3 manipulation. In addition, we use live imaging of +TIP and MT behaviors to explore the effects of TACC3 manipulation on MT plus end dynamics within living growth cones, as well as within other embryonic cell types. Finally, we examine the interaction of TACC3 with XMAP215 on the plus ends of MTs in interphase embryonic cells. These analyses highlight new insights into the function of TACC3 and how it regulates MT plus end dynamics.

RESULTS

TACC3 protein is expressed within embryonic neuronal growth cones and promotes axon outgrowth

We first performed immunostaining of fixed, cultured embryonic neural crest cells and neuronal growth cones, using an antibody specific to *X. laevis* TACC3. Within neural crest cells, we observed punctate staining throughout the entire cell (Figure 1, A–C), as well as staining at the centrosome (Figure 1, A′–C′), consistent with previous reports of TACC3 localization (Gergely *et al.*, 2000b; Groisman *et al.*, 2000). We also observed strong labeling within axons and growth cones (Figure 1, D–F), which has not been previously reported, and we confirmed TACC3 presence in neural tissue by Western blot of axon lysates (Figure 1 Supplement). These results suggest that TACC3 may play a role within the growth cone during axon outgrowth.

To investigate whether TACC3 functions during axonal development, we examined the extent of axon outgrowth of cultured neurons after manipulation of TACC3 levels. An antisense morpholino oligonucleotide (MO) directed against the TACC3 start site inhibited TACC3 expression (Figure 1G) and reduced both axonal number and axonal length (Figure 1, H–K). TACC3 overexpression (OE) did not affect axonal number but did result in significant increase in axonal length (Figure 1, L–P). Thus our findings suggest that TACC3 may play a critical role during embryonic nervous system development and indicate that normal levels of TACC3 are required for proper axonal outgrowth.

TACC3 regulates MT plus end dynamics in growth cones and other cell types

Axon outgrowth is regulated in large part by MT dynamics within the neuronal growth cone, which is the dynamic structure at the tip of the growing axon (Tanaka *et al.*, 1995; Lowery and Van Vactor, 2009). Thus we sought to examine whether MT plus end dynamics were specifically disrupted within growth cones after TACC3 manipulation. To test this, we acquired high-resolution live images of tagged end-binding protein 1 (EB1), which binds all growing MT plus ends (Stepanova *et al.*, 2003), and we then quantified parameters of MT polymerization dynamics using the Matlab-based open-source software plusTipTracker (Applegate *et al.*, 2011). This software program has been validated for accurate tracking of EB1-GFP comets in *X. laevis* growth cones, using identical imaging conditions to those used in the present study (Stout *et al.*, 2014). EB1-GFP comet number and morphology were similar in control, TACC3 knockdown (KD), and TACC3 OE growth cones (Figure 2, A–C, and Figure 2 Supplemental Movies 1–4). However, compared with controls, EB1-GFP comet velocity was reduced by 11% upon TACC3 KD and increased by 11% upon TACC3 OE (Figure 2D). MT growth-track lifetime (which measures the number of seconds of MT polymerization in a given growth track before pausing or catastrophe) was not affected by TACC3 manipulation (Figure 2E). Conversely, MT growth-track length (which measures the distance of persistent MT polymerization growth before pausing or catastrophe) was significantly decreased in KD and increased in OE. TACC3 KD led to a 14% reduction in MT growth-track length, whereas TACC3 OE led to an 18% increase in MT growth-track length (Figure 2F). To summarize, although the time persistence of MT polymerization is independent of TACC3, the velocity and length of MT forward progression trend with the level of TACC3, suggesting that TACC3 promotes more efficient MT polymerization.

To determine whether TACC3 regulation of MT dynamics is specific to neuronal growth cones, we also examined the effect of TACC3 manipulation in cultured embryonic neural crest cells. In these cells, we saw a similar effect to that which occurred within growth cones. There were reductions in MT growth velocity and length with TACC3 KD and increases in velocity and length with TACC3 OE (Figure 2, G and I), whereas there was no effect on MT growth lifetime (Figure 2H). Taken together, our results demonstrate that TACC3 regulates MT plus end dynamics in motile vertebrate interphase cells.

TACC3 can act as a +TIP in neuronal growth cones and other primary embryonic cell types

To gain further insight into how TACC3 mechanistically affects MT plus end behaviors, we examined the subcellular dynamics of

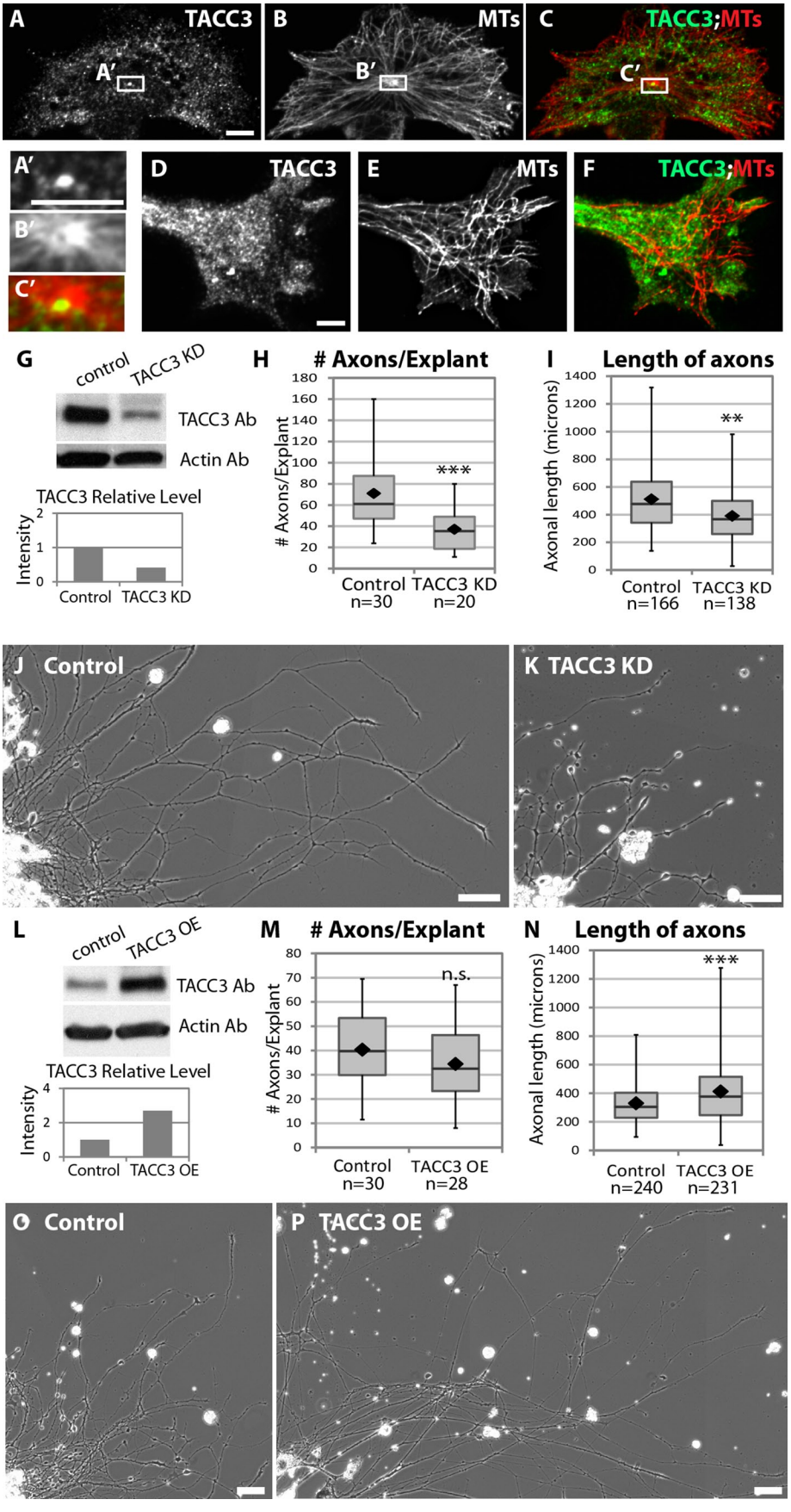

FIGURE 1: TACC3 protein is expressed within embryonic neuronal growth cones and promotes axon outgrowth. (A–F) Immunostaining with antibodies to TACC3 (A) and tubulin (B) in cultured embryonic neural crest cells confirm that TACC3 is enriched at the centrosome (C, A′–C′), in addition to being present in puncta throughout the cell. (D–F) TACC3 antibody also strongly stains growth cones. Scale bar, 5 μm. (G) Western blot showing that a morpholino (MO) targeted against TACC3 results in 50% knockdown (KD) by 2 d postfertilization. Bar graph depicts densitometry of blot shown; however, similar results were obtained with >20 individual Western blots (unpublished data). (H–I) Axon outgrowth parameters after 24 h in culture were quantified in control and TACC3 KD conditions. (H) The numbers of axons per neural tube explant were counted from three independent experiments. (I) The distance from explant to growth cone was measured to calculate the length of axons from three independent experiments. (J–K) Representative phase contrast microscopy images of axons from control and TACC3 KD. (L) Western blot showing that TACC3 levels are increased (overexpressed [OE]) 2 d after injecting embryos with TACC3 mRNA. Bar graph depicts densitometry of blot shown; however, similar results were obtained with >20 individual Western blots (unpublished data). Note that the TACC3 blot in L was exposed for a shorter amount of time than the one in G, which explains the fainter control band in L. (M, N) Axon outgrowth parameters after 18 h in culture were quantified in control and TACC3 OE conditions. (O–P) Representative phase contrast microscopy images of axons from control and TACC3 OE. Box-and-whisker plots indicate the mean (diamond), median, extrema, and quartiles. An unpaired *t* test was performed to assess significance between conditions. $^{**}p < 0.01$, $^{***}p < 0.001$; n.s., not significant. Bar, 50 μm (J, K, O, P).

TACC3 within living embryonic cells. Thus we tagged full-length TACC3 with GFP and examined its localization within both growth cones and neural crest cells (Figure 3 and Figure 3 Supplemental Movies 1–3). GFP-tagged TACC3 strongly localized to the growing plus ends of MTs in both cell types (Figure 3, A–C and G–I). In growth cones, the mean length of the GFP-TACC3 plus end accumulation was ~0.70 μm (Figure 3, D and E; data measured from 70 MTs). GFP-TACC3 was primarily detected on MT plus ends that either appeared to be advancing forward or paused, with 100% of growing MTs displaying detectable GFP-TACC3 plus end localization (Figure 3F). Seventy-seven percent of paused MTs still showed GFP-TACC3 localization, whereas 25% of shrinking MTs also had observable GFP-TACC3 localization. These observations were similar in neural crest cells, although the GFP-TACC3 comets were shorter, with a mean length of 0.53 μm (Figure 3, J and K; data measured from 64 MTs). GFP-TACC3

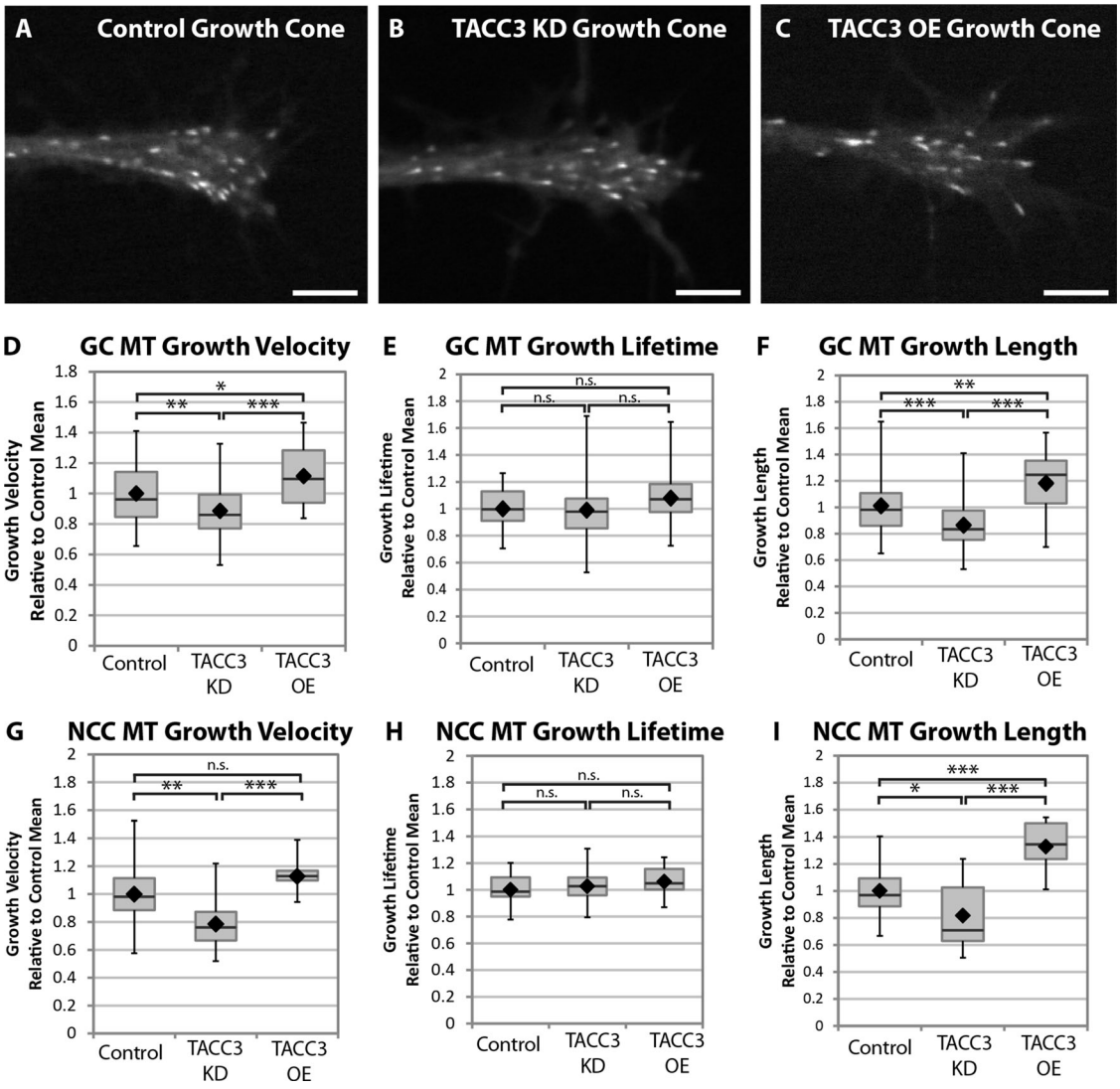

FIGURE 2: TACC3 regulates MT dynamics in *X. laevis* growth cones and neural crest cells. (A–C) Representative micrographs of EB1-GFP comets in control (A), TACC3 KD (B), and TACC3 OE (C) conditions. See Figure 2 Supplemental Movies S1–S4. Bar, 5 µm. (D–F) Quantification of MT growth track parameters in cultured embryonic neuronal growth cones (GC) after TACC3 manipulation. EB1-GFP localizes to the ends of growing MTs and is thus a marker for MT polymerization. Automated tracking of EB1-GFP comets calculate MT growth-track velocity (D), MT growth-track lifetime (E), and MT growth-track length (F). Examples of actual mean values for a single experiment: GC MT velocity, control, 6.4 µm/min; TACC3 KD, 5.7 µm/min; TACC3 OE, 7.1 µm/min. GC MT lifetime, control, 12.6 s; KD, 13.3 s; OE, 14.1 s. GC MT length, control, 1.4 µm; KD, 1.3 µm; OE, 1.7 µm. NCC MT velocity, control, 7.5 µm/min; KD, 6.0 µm/min; OE, 8.5 µm/min. NCC MT lifetime, control. 11.4 s; KD. 13.0 s; OE, 12.1 s. NCC MT length, control, 1.3 µm; KD, 1.3 µm; OE, 1.8 µm. For each independent experiment (six were performed in total), measurements of MT parameters were normalized to their respective experimental control means due to the significant day-to-day fluctuations in control MT dynamics (in part, due to room temperature changes). Control data represent the means of 44 growth cones, representing a total of 1228 analyzed tracks; TACC3 KD represents 49 growth cones with 964 tracks; TACC3 OE represents 24 growth cones with 524 tracks. (G–I) Quantification of MT growth-track parameters in cultured embryonic neural crest cells. Control data represent the means of 20 neural crest cells, representing a total of 2876 analyzed tracks; TACC3 KD represents 13 cells with 1313 tracks; TACC3 OE represents 10 cells with 1386 tracks. Box-and-whisker plots indicate the mean (diamond), median, extrema, and quartiles. An unpaired *t* test was performed to assess significance between conditions. *$p < 0.05$, **$p < 0.01$, ***$p < 0.001$; ns, not significant.

accumulation was detectable on 100% of growing MTs, 69% of paused MTs, and 25% of shrinking MTs (Figure 3L). Thus we find that GFP-TACC3 robustly tracks plus ends of MTs in vertebrate growth cones and neural crest cells.

Plus end tracking of GFP-TACC3 was not restricted to neural-derived cells, as fibroblasts isolated from mesodermal somite tissue also showed clear plus end tracking (Figure 4, A–C, and Figure 4 Supplemental Movies 1 and 2). We also observed on several occasions that shrinking MTs paused concurrently with obvious accumulation of GFP-TACC3 (Figure 4D). This was most apparent in the mesodermal and neural crest cells, as these had greater numbers of MTs to examine. The plot profiles and distribution of GFP-TACC3 on

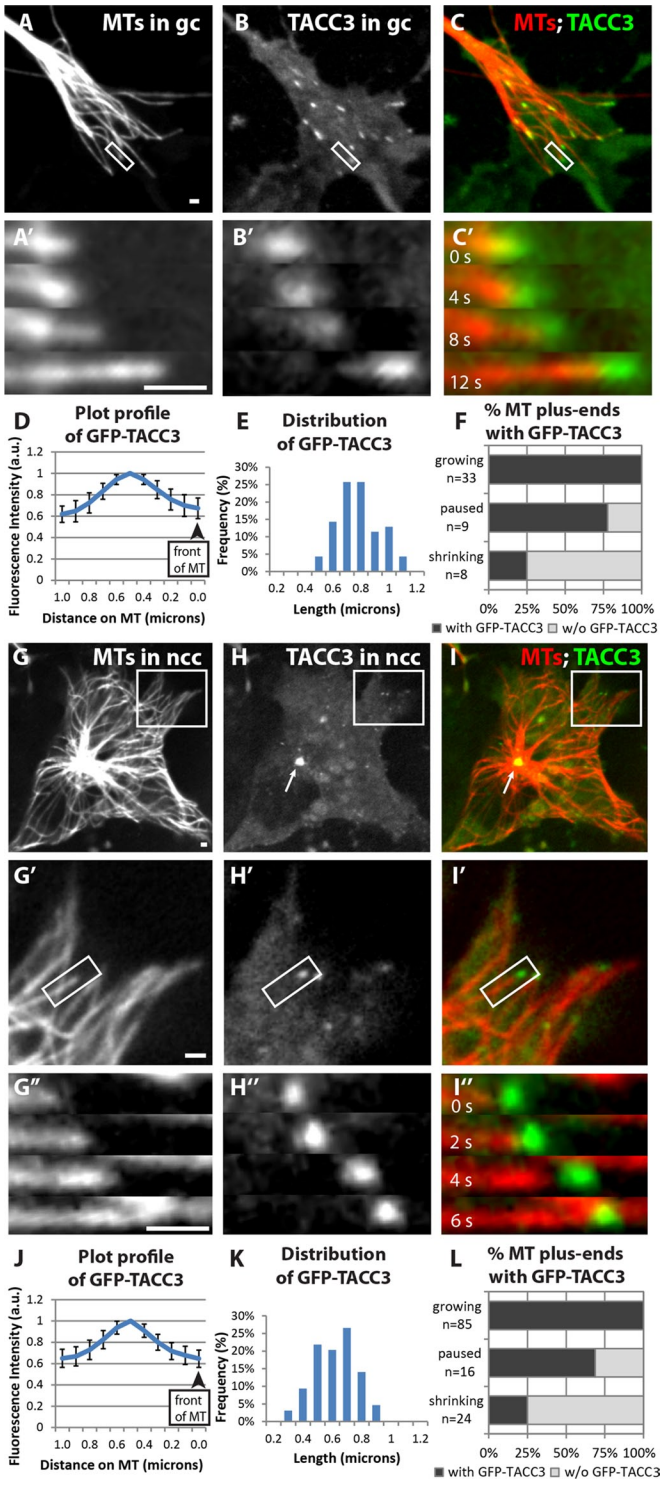

FIGURE 3: TACC3 can act as a +TIP in neuronal growth cones and neural crest cells. (A–C) Expression of mKate2-tubulin (A), GFP-TACC3 (B), and merge (C) in living growth cone (gc). See Figure 3 Supplemental Movie 1. (A′–C′) Magnified time-lapse montages of the boxed regions in A–C shows that GFP-TACC3 localizes to growing MT plus ends. (D) Fluorescence intensity profile of line-scan average from 30 MT plus ends in growth cones. (E) Histogram depicting the distribution of lengths of detectable GFP-TACC3 localization on the plus ends of MTs in growth cones. (F) Percentage of MT plus ends with GFP-TACC3 localization for different MT dynamics instability states. (G–I) Expression of mKate2-tubulin (G), GFP-TACC3 (H), and merge (I) in living neural crest cell (ncc). See Figure 3 Supplemental Movie 2. (G′–I′) Magnified views of the boxed regions in G–I. See Figure 3 Supplemental Movie 3. (G″–I″) Magnified time-lapse montages of the boxed regions in G′–I′. (J) Fluorescence intensity profile of line-scan average from 45 MT plus ends in neural crest cells. (K) Distribution of lengths of detectable GFP-TACC3 localization on the plus ends of MTs. (L) Percentage of MT plus ends with GFP-TACC3 localization for different MT dynamics instability states. Bar, 1 μm.

MT plus ends in fibroblasts were similar to that of the neural cell types, with mean length of GFP-TACC3 plus end accumulation being 0.67 μm (Figure 4, E and F, data measured from 55 MTs). GFP-TACC3 accumulation was detectable on 100% of growing MTs, 70% of paused MTs, and 25% of shrinking MTs (Figure 4G; see also Figure 4 Supplement for an example of GFP-TACC3 on shrinking MT). Measuring fluorescence intensity values of GFP-TACC3 localized at the tips of MTs demonstrated that whereas GFP-TACC3 was observable on one-fourth of shrinking MTs (Figure 4G), mean GFP intensities were ~40% less on shrinking MTs than on growing MTs. In addition, the maximum intensity of GFP-TACC3 fluorescence on shrinking MTs (106 fluorescence units; top whisker in Figure 4H, box plot) was close to half that of the maximum intensity of fluorescence on growing MTs (172 fluorescence units; Figure 4H), demonstrating that the maximum number of GFP-TACC3 molecules that localize to shrinking MTs is not as great as those that can bind to growing MT plus ends. Thus our results demonstrate that TACC3 can act as a +TIP in multiple vertebrate embryonic cell types and also support the notion that TACC3 may either promote MT polymerization or reduce MT catastrophe.

TACC3 requires its TACC domain for MT plus end tracking

To determine the plus end tracking mechanism of TACC3, we constructed several structural domain mutants of TACC3 (Figure 5A). Full-length GFP-TACC3 accumulates at all growing MT plus ends, as designated by mKate2-EB1 comets (Figure 5B and Figure 5 Supplemental Movie 1). Deleting the highly conserved N-terminal domain did not prevent plus end tracking (Figure 5, E–G, and Figure 5 Supplemental Movie 2). However, it did result in longer GFP-TACC3 plus end comets compared with controls, as well as longer EB1-GFP comets (Figure 5, E and F, and Figure 5 Supplemental Movie 2). These data suggest that the conserved N-terminal domain is involved in restricting TACC3 to the extreme plus end and also that TACC3 localization may affect EB1 binding to MT plus ends as well. Conversely, removing either the entire TACC domain (unpublished data) or even just the second coiled-coil domain of the TACC domain completely abrogated MT plus end tracking (Figure 5, H–J, and Figure 5 Supplemental Movie 3), demonstrating that the TACC domain, and in particular the second coiled-coil domain, is essential for TACC3 plus end tracking. We then observed significant interference with plus end tracking ability when TACC3 was tagged with GFP on the C-terminal end (Figure 5, K–M, and Figure 5 Supplemental Movie 4), further supporting the importance of the TACC domain for plus end tracking. However, whereas the TACC domain is necessary for promoting plus end tracking, it is not sufficient, as the entire TACC domain alone did not localize to MT plus ends (Figure 5, N–P, and Figure 5 Supplemental Movie 4).

TACC3 localization on MT plus ends is more distal than EB1 and overlaps with XMAP215

It is well established that the growing end of a MT is home to many different +TIPs, including EB1, CLASP, and XMAP215 (Akhmanova

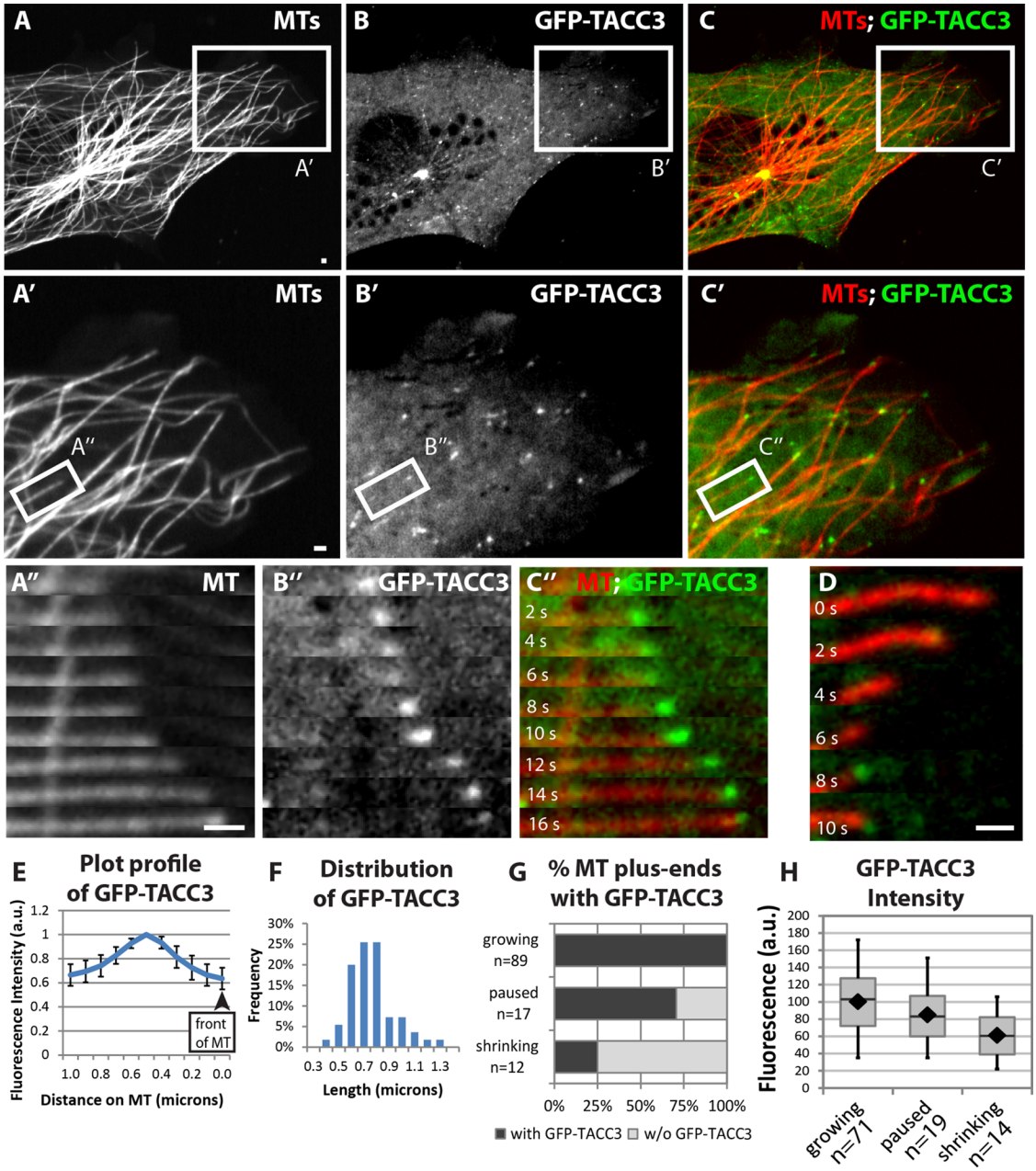

FIGURE 4: TACC3 can act as a +TIP in nonneuronal embryonic cells. (A–C) Expression of mKate2-tubulin (A), GFP-TACC3 (B), and merge (C) in cultured fibroblasts derived from embryonic somitic mesoderm. See Figure 4 Supplemental Movie 1. (A′–C′) Magnified views of the boxed regions in A–C. See Figure 4 Supplemental Movie 2. (A″–C″) Magnified time-lapse montages of the boxed regions in A′–C′. (D) Time-lapse montage of another MT in the process of undergoing catastrophe, with GFP-TACC3 localizing. (E) Fluorescence intensity profile of line-scan average from 43 MT plus ends. (F) Histogram depicting the distribution of lengths of detectable GFP-TACC3 localization on the plus ends of MTs. (G) Percentage of MT plus ends with GFP-TACC3 localization for different MT dynamics instability states. (H) Quantification of mean fluorescence intensity of 4 × 4 pixel square of GFP-TACC3 accumulation on the ends of MTs, when visible. Box-and-whisker plots indicate the mean (diamond), median, extrema, and quartiles. Bar, 1 μm.

and Steinmetz, 2008). Different +TIPs have overlapping yet unique localizations on the ends of the MTs, depending on their particular binding affinities. XMAP215 is known as the distalmost +TIP, and EB1 is located directly behind it on MTs (Nakamura *et al.*, 2012; Maurer *et al.*, 2014). Most other +TIPs, including CLASP, partially overlap with EB1 and trail further behind it (Hur *et al.*, 2011). Because the fly orthologue of TACC3 genetically interacts with CLASP (Long *et al.*, 2013), yet TACC3 biochemically interacts with XMAP215 (Kinoshita *et al.*, 2005; O'Brien *et al.*, 2005; Peset *et al.*, 2005), we examined where TACC3 specifically localized on the MT plus end. We performed sequential imaging of red and green channels in both time orders to compare colocalizations between the two proteins. Although this type of dual-image-comparison analysis allowed for the analysis of colocalization dynamics, we also calculated the frame-to-frame velocity of the growing MT plus end in order to account for the 1-s time delay between channels for each examined

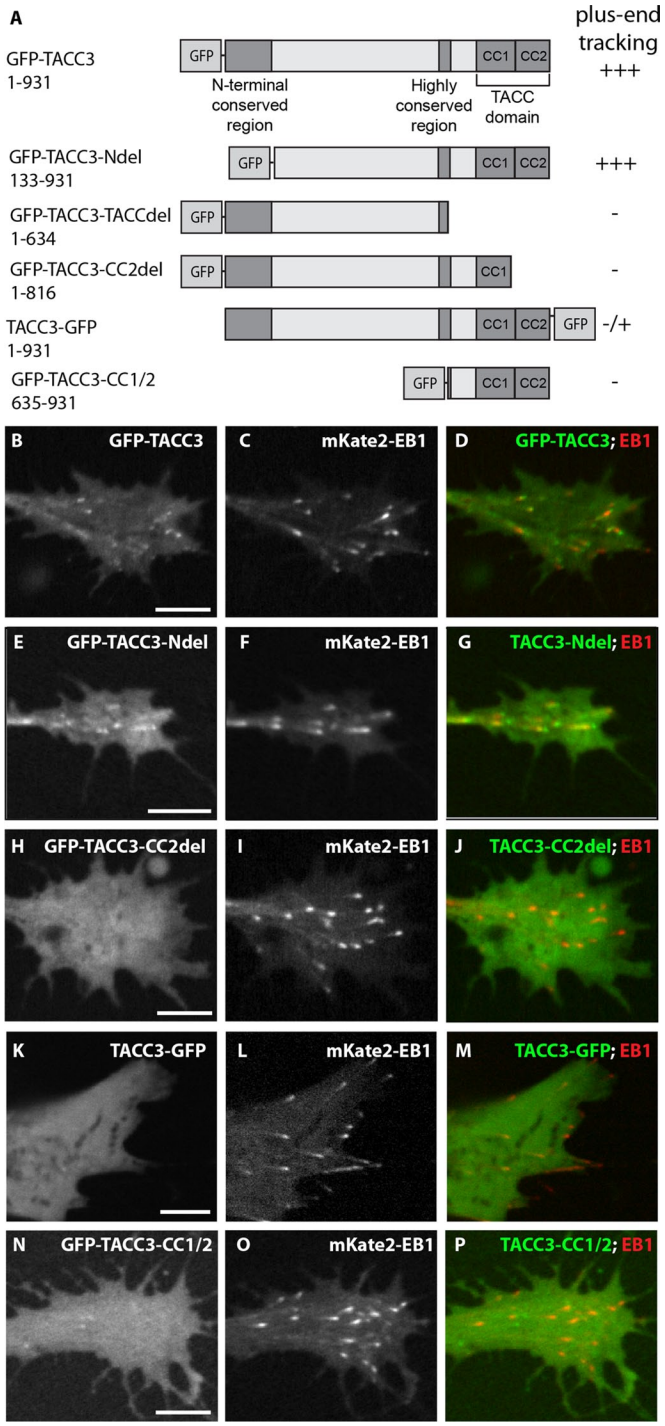

FIGURE 5: The TACC domain is necessary but not sufficient for MT plus end tracking by TACC3. (A) Schematic representation of GFP-tagged TACC3 proteins and deletion constructs, and designation of whether the protein tracks along growing MT plus ends. The amino acid residue numbers refer to those in full-length *X. laevis* TACC3 from GenBank accession number NP_001081964.1. Conserved domains of TACC3 include an N-terminal, conserved region, a C-terminal, highly conserved TACC domain, and a short, highly conserved region, which is located before the TACC domain. The TACC domain consists of two coiled-coil (CC) domains, CC1 and CC2. The TACC domain is necessary for localization to the centrosome (Gergely *et al.*, 2000b; Peset *et al.*, 2005) and interaction with XMAP215 family members (Lee *et al.*, 2001; Thakur *et al.*, 2014). (B–M) Expression of GFP-tagged TACC3 constructs (B, E, H, K, N), mKate2-EB1 (to identify MT plus ends; C, F, I, L, O), and merged images of both channels (D, G, J, M, P). Plus end accumulation is apparent in B and E but not H, K, or N. Images in K–M are from the edge of a neural crest cell, whereas all others are growth cones. See Figure 5 Supplemental Movies 1–5. Bar, 5 μm.

MT and used these measurements to translate one channel in the *x*-axis to obtain the final images in Figure 6. We also used these time-corrected images for measuring approximate distances between peak intensity values.

We found that TACC3 partially overlaps with, but is distal to, EB1 (Figure 6, A–C), with a distance of ~0.5 μm between the peak fluorescence intensity profiles of the GFP-TACC3 versus the mKate2-EB1 line scans (Figure 6D). No matter which channel was imaged first (red or green), TACC3 was always distal to EB1, clearly demonstrating that even without correcting for the time delay, TACC3 lies distal to EB1.

Moreover, when we analyzed the colocalization of tagged TACC3 and tagged XMAP215, we found that they directly overlapped each other (Figure 6, E–G), with an almost identical fluorescence intensity plot profile (Figure 6H). Because TACC3 and XMAP215 directly overlap, the fluorophore that corresponded to the second channel imaged was always distal to the other (before translation correction). Translation based on plus end velocity led to complete juxtaposition of the two puncta. Taken together, these data suggests that TACC3 is at the extreme MT plus end, an ideal position from which to directly regulate MT polymerization by XMAP215.

TACC3 and XMAP215 affect each other's protein stability and localization to MT plus ends

Colocalization of XMAP215 and TACC3 suggests that they may interact at the MT plus end, consistent with their binding in vitro (Kinoshita *et al.*, 2005; O'Brien *et al.*, 2005; Peset *et al.*, 2005). Because TACC3 localizes XMAP215 orthologues to centrosomes (Cullen and Ohkura, 2001; Lee *et al.*, 2001; Bellanger and Gonczy, 2003; Le Bot *et al.*, 2003; Srayko *et al.*, 2003; O'Brien *et al.*, 2005), we wondered whether TACC3 was also participating in localizing XMAP215 to MT plus ends in embryonic cell types. In addition, since the worm orthologues of TACC3 and XMAP215 are dependent on each other for overall cytoplasmic stability (Bellanger and Gonczy, 2003), we questioned whether this stabilizing activity also occurred with TACC3 and XMAP215 in vertebrate cells.

First, we determined that manipulating overall TACC3 protein levels had a corresponding effect on XMAP215 protein levels in whole embryo lysates. As TACC3 levels were reduced, XMAP215 levels decreased (Figure 7A), whereas adding back TACC3 mRNA to the TACC3 KD rescued XMAP215 levels (Figure 7A). Consistently, overexpressing TACC3 led to increased levels of XMAP215 (Figure 7B). Furthermore, TACC3 levels appeared depend on XMAP215 as well, because reducing XMAP215 led to a reduction in TACC3 protein (Figure 7C). Of note, overexpressing TACC3 in the XMAP215 KD background partially rescued the reduction in XMAP215 levels (Figure 7C'), consistent with a function for TACC3 in stabilizing XMAP215 protein. Alternatively, because TACC3 is a known translation regulator (Stebbins-Boaz *et al.*, 1999), TACC3 could be increasing XMAP215 levels by increasing its protein synthesis. However, increased XMAP215 levels also had a positive effect on TACC3 levels (Figure 7D).

We then tested whether TACC3 levels correlated with changes in XMAP215 localization on MT plus ends. Knocking down TACC3 by 50% led to a small (11%) yet significant reduction in XMAP215-GFP

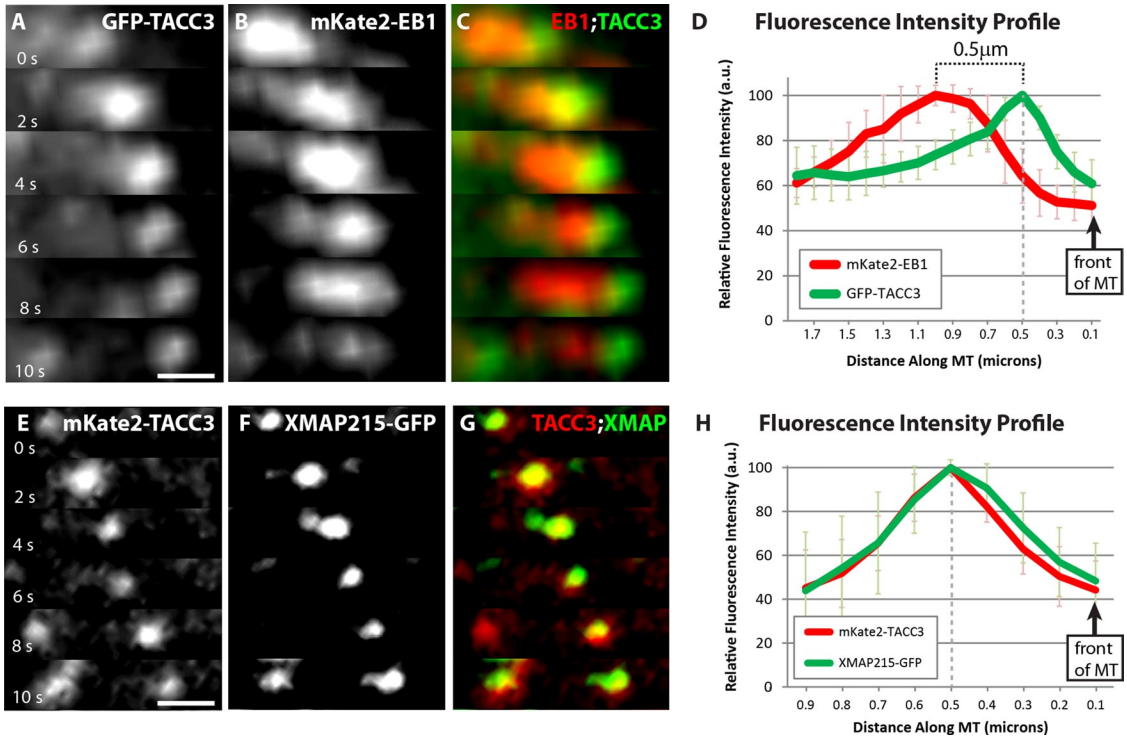

FIGURE 6: TACC3 localization on MT plus ends is more distal than EB1 and overlaps with XMAP215. (A–C) Representative time-lapse montage of GFP-TACC3 (A) and mKate2-EB1 (B) accumulation on growing MT plus end. MT is growing to the right. Merged image (C) highlights the spatial arrangement between GFP-TACC3 and mKate2-EB1 localizations. These images were compiled by translating the TACC3 channel on the *x*-axis, after calculating the frame-to-frame velocity of the growing MT plus end, in order to account for the 1-s time delay between channels, for each examined MT (using ImageJ Translate function). To further confirm correct translation, uncorrected time-lapse colocalizations were examined with both combinations of imaging—red channel first, green channel second; then green channel first, red channel second. (D) Fluorescence intensity profiles of GFP-TACC3 and mKate2-EB1. GFP-TACC3 and mKate2-EB1 signals from 12 individual MTs were quantified by intensity line scans to present the relative fluorescence intensity profiles, with the plus end of the MT toward the right. The highest-intensity peak of GFP-TACC3 is ~0.5 μm distal to the peak of mKate2-EB1. (E–G) Representative time-lapse montage of mKate2-TACC3 (E) and XMAP215-GFP (F) accumulation on growing MT plus end. MT is growing to the right. Merged image (G) shows that mKate2-TACC3 and XMAP215-GFP localizations overlap. (H) Fluorescence intensity profiles of mKate2-TACC3 and XMAP215-GFP. mKate2-TACC3 and XMAP215-GFP signals from 11 individual MTs were quantified by intensity line scans to present the relative fluorescence intensity profiles. Note that peak intensities of mKate2-TACC3 and XMAP215-GFP closely align. Bar, 0.5 μm.

fluorescence intensity on MT plus ends (Figure 7E). TACC3 OE resulted in a 14% increase of XMAP215-GFP levels on MT plus ends (Figure 7E). These results suggest that TACC3 may indeed be involved in localizing, or maintaining, XMAP215 on MT plus ends. Of interest, reducing XMAP215 levels also leads to mildly reduced GFP-TACC3 localization (by 8%) on MT plus ends (Figure 7F).

DISCUSSION

TACC3 is a +TIP that regulates microtubule plus end dynamics

There has been speculation that TACC-family proteins may regulate MT plus end dynamics (Peset and Vernos, 2008), because the length of centrosomal MTs correlates with the level of TACC3 in multiple systems (Gergely *et al.*, 2000b; Bellanger and Gonczy, 2003; Le Bot *et al.*, 2003; Srayko *et al.*, 2003; Kinoshita *et al.*, 2005; O'Brien *et al.*, 2005). Moreover, studies performed in *Drosophila* and *Dictyostelium* showed that TACC-domain family members track along growing MT plus ends (Lee *et al.*, 2001; Samereier *et al.*, 2011). However, in vertebrates, TACC3 localization was believed to be restricted to the centrosome and mitotic spindle, based on TACC3 immunostaining of fixed cells (Groisman *et al.*, 2000; O'Brien *et al.*, 2005). It has been difficult to rationalize the localization of TACC3 at the centrosome with its effects on MT length, because length is primarily controlled by events at the MT plus end.

One study examined whether vertebrate TACC3 bound specifically to MT plus ends (O'Brien *et al.*, 2005), but this study used an indirect method of testing whether TACC3 displayed an increased affinity for experimentally sheared MTs (which presumably have more plus ends) using an in vitro assay. However, sheared MT ends would have abnormal MT plus end structures and are not in the process of growing. Because the definition of a +TIP is a protein that tracks along growing MT ends, the most reliable method for defining a +TIP is to examine its potential localization on growing MT plus ends.

In this study, we expressed GFP-TACC3 and observed its behavior in living vertebrate growth cones, neural crest cells, and mesodermal fibroblasts, and we found that GFP-TACC3 localizes to MT plus ends in all cell types examined. We note that immunostaining did not show plus end localization, but a likely reason is that TACC3 is released from plus ends during fixation (unpublished data). Thus this study provides the first evidence that vertebrate TACC3 can directly regulate MT plus end dynamics by functioning as a +TIP.

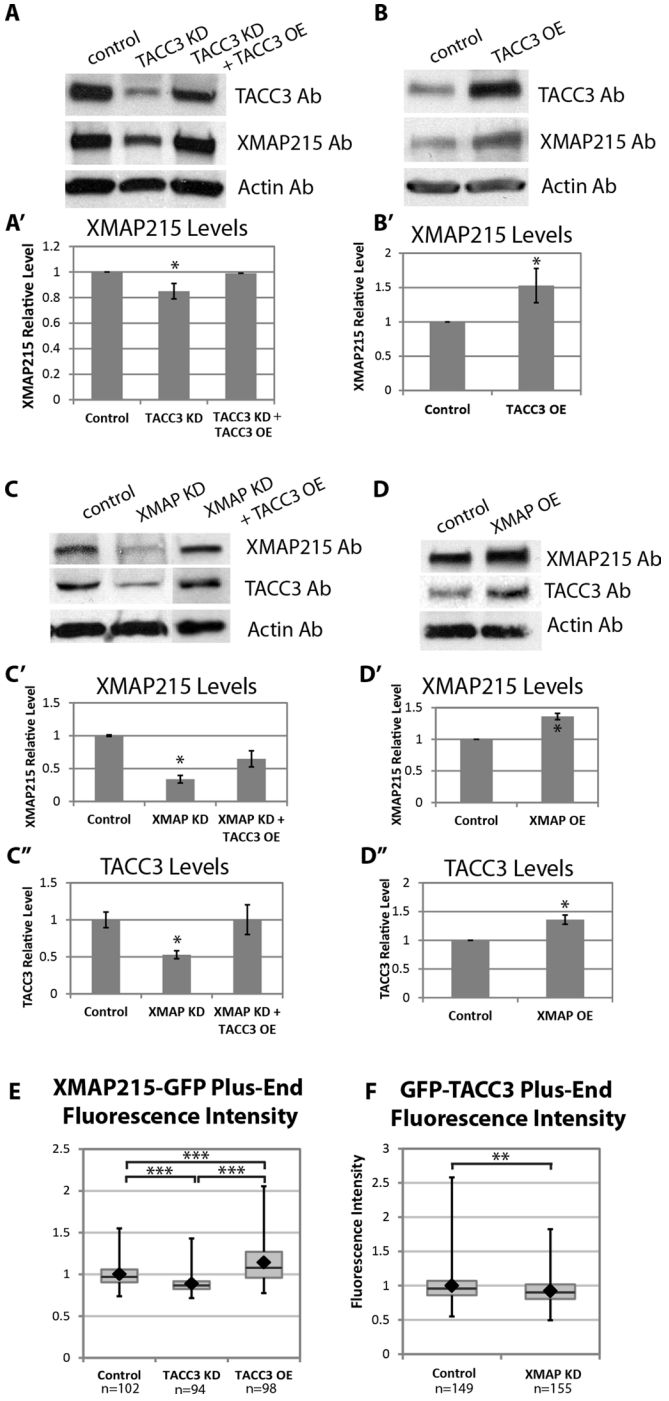

FIGURE 7: TACC3 and XMAP215 levels affect each other's protein stability and localization to MT plus ends. (A, B) Representative Western blots showing levels of TACC3 and XMAP215 after TACC3 KD (A) or overexpression (B). The graphs in A′ and B′ are compilations of seven and six individual Western blot experiments, respectively. (C, D) Representative Western blots showing levels of XMAP215 and TACC3 after XMAP215 KD (C) or overexpression (D). The graphs in C′ and C″ are from six Western blot experiments, and D′ and D″ are from three experiments. Bars in graphs of Western densitometry denote SE. A Kruskal–Wallis test was performed to assess significance of differences in Western blot densitometry. *$p < 0.05$.
(E) Quantification of fluorescence intensity levels of XMAP215-GFP on MT plus ends in control, TACC3 KD, and TACC3 OE conditions, normalized to cytoplasmic levels. Data represent analysis of ~100 individual MTs from numerous growth cones for each condition.
(F) Quantification of fluorescence intensity levels of GFP-TACC3 on MT plus ends in control and XMAP215 KD conditions, normalized to cytoplasmic levels. Data represent analysis of 149 and 151 individual MTs from numerous growth cones per condition. Box-and-whisker plots indicate the mean (diamond), median, extrema, and quartiles. An unpaired *t* test was performed to assess significance between conditions. **$p < 0.01$, ***$p < 0.001$; ns, not significant.

Previous studies in *Drosophila* and *Dictyostelium* also showed that the highly conserved C-terminal TACC domain was responsible for plus end tracking (Lee *et al.*, 2001; Samereier *et al.*, 2011). Our observations with *X. laevis* TACC3 demonstrate that this function of the TACC domain is well conserved.

Interactions between TACC3 and XMAP215

It is well established that TACC3 and XMAP215 family members interact in vitro and that TACC3 is required for XMAP215 localization to the centrosome (Cullen and Ohkura, 2001; Lee *et al.*, 2001; Bellanger and Gonczy, 2003; Le Bot *et al.*, 2003; Srayko *et al.*, 2003; O'Brien *et al.*, 2005; Kinoshita *et al.*, 2005; Peset *et al.*, 2005). However, it had been unclear whether TACC3 localizes with XMAP215 at MT plus ends as well. In our study, we demonstrate that TACC3 and XMAP215 do interact at MT plus ends and that this interaction is likely important for regulating MT growth dynamics.

As TACC3 interacts in vitro with XMAP215 family members through the TACC domain (Lee *et al.*, 2001; Thakur *et al.*, 2014), and since we determined that the TACC domain is also required for MT plus end tracking, it is possible that TACC3 is recruited to MT plus ends through interaction with XMAP215. However, knocking down TACC3 also reduces XMAP215 plus end localization and vice versa. These results suggest that each is required for the other's normal localization to plus ends. It was previously suggested that TACC3 might enhance the affinity of XMAP215 for MTs, as a 1:1 TACC3-XMAP215 complex allows more XMAP215 to bind to MTs than XMAP215 alone (Kinoshita *et al.*, 2005; Peset *et al.*, 2005). Thus TACC3 interaction with XMAP215 may promote XMAP215 binding to plus ends, driving more efficient MT polymerization. This is supported by our finding that TACC3 OE leads to significantly more XMAP215 accumulation on plus ends, and this extra XMAP215 may account for the faster MT growth velocities that we observe with TACC3 OE (Figure 2D). It is worth noting that two other +TIPs have recently been described that also promote the recruitment of XMAP215 orthologues to MT plus ends: SLAIN2 in mammalian cells (van der Vaart *et al.*, 2011, 2012) and Sentin in *Drosophila* (Li *et al.*, 2011). Thus it appears that the regulation of XMAP215 on MT plus ends is becoming increasingly complicated.

Evidence suggests that the TACC3-XMAP215 complex may generally be more stable than either protein individually, as each of them affects the protein level of the other in *Xenopus* whole-embryo lysates. This is consistent with studies in *Caenorhabditis elegans* showing that normal levels of TACC3 and XMAP215 orthologues are required to maintain the overall cytoplasmic signal of the other (Bellanger and Gonczy, 2003). Taken together, our data combined with others suggest a model in which XMAP215 and TACC3 form a complex in the cytoplasm that reduces protein turnover and also may increase their binding efficiency to MT plus ends, thus driving more effective MT polymerization (Figure 8). However, we also note that *Xenopus* TACC3 was first identified as a protein (originally named Maskin) that associates with CPEB to regulate translation in the oocyte (Stebbins-Boaz *et al.*, 1999), and so it is also possible that TACC3 could be regulating XMAP215 protein synthesis rather than, or in addition to, protein stability.

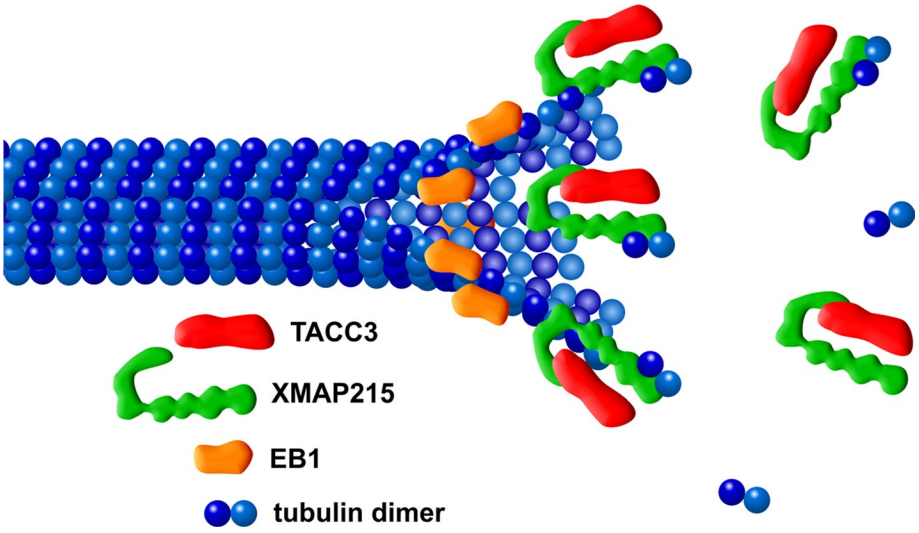

FIGURE 8: Cartoon schematic of proposed model of TACC3 interaction at MT plus ends. Both TACC3 (red) and XMAP215 (green) bind to the extreme MT plus end. TACC3 and XMAP215 are known to interact with each other through their C-terminal domains (Lee *et al.*, 2001; Thakur *et al.*, 2014), whereas XMAP215 can bind to tubulin dimers through its N-terminal TOG domains (Widlund *et al.*, 2011). TACC3 and XMAP215 complex formation in the cytoplasm may serve to stabilize each other (Bellanger and Gonczy, 2003; Figure 7), and TACC3 interaction with XMAP215 may promote more efficient binding of the complex to MTs in order to drive MT polymerization activity (Kinoshita *et al.*, 2005; Peset *et al.*, 2005). It is unknown whether TACC3 can bind to MT plus ends directly or only through XMAP215 (as depicted here). EB1 (orange) binding to MT plus ends is behind TACC3 and XMAP215 (Figure 6). Not drawn to scale.

TACC3 and XMAP215 are the only two +TIPs known to localize at the extreme MT plus end to drive MT polymerization. Unlike EB1-GFP, which binds solely to growing MT plus ends, GFP-TACC3 can also bind to paused and even shrinking MTs (albeit at a lower frequency and intensity compared with growing MTs). Although this is unusual for a +TIP, there is precedence for another +TIP (XMAP215) that tracks shrinking plus ends in vivo (Lowery *et al.* 2013). Although it is possible that this backtracking is due to exogenous expression of the GFP-TACC3 construct, it also could be that TACC3 recognizes a structural conformation that is present at both growing and shrinking MT plus ends. Moreover, many +TIPs contain SxIP motifs that facilitate interaction with EB proteins for recruitment to growing MT plus ends (Honnappa *et al.*, 2009). We were unable to find an SxIP motif within the TACC domain; however, there is a SxIP-like motif (SPLPIP) at amino acid 311 that may contribute to plus end recruitment. The exact mechanism by which TACC3 tracks along plus ends, and whether it requires XMAP215 or EB1, is an important question for the future.

TACC3 regulates axon outgrowth

Axon outgrowth is regulated in part by microtubule polymerization (Tanaka *et al.*, 1995; Lowery and Van Vactor, 2009), which is in turn controlled by +TIPs (Akhmanova and Steinmetz, 2008). Yet only a handful of +TIPs have been functionally implicated within the neuronal growth cone (Lee *et al.*, 2004; Zhou *et al.*, 2004; Hur *et al.*, 2011; Neukirchen and Bradke, 2011; Lowery *et al.*, 2013). Our study shows that TACC3 also functions as a +TIP within the growth cone and that manipulation of TACC3 levels leads to corresponding changes in axonal outgrowth. Given that these changes correlate with similar alterations in microtubule polymerization rates within growth cones (Figure 2), it is possible that TACC3 regulates axonal outgrowth by regulating microtubule polymerization rates. This is partially supported by the classic findings that disrupting MT dynamics with low levels of MT-depolymerizing drugs also results in reduced axon outgrowth (Tanaka *et al.*, 1995; Rochlin *et al.*, 1996). However, the role of TACC3, and +TIPs in general, in promoting axon outgrowth is likely much more sophisticated than simply controlling the rates of polymerization. It has also been suggested that some +TIPs regulate how MTs interact with F-actin in growth cones (e.g., Engel *et al.*, 2014), and future studies may uncover whether TACC3 plays a role in this as well.

In conclusion, we used live imaging in cultured embryonic cells to demonstrate that vertebrate TACC3 regulates specific aspects of microtubule growth dynamics. We show that TACC3 can function as a +TIP, closely overlapping with XMAP215 at the extreme MT plus end. We also establish a role for TACC3 in the promotion of axonal outgrowth. Because TACC3 localization is controlled by phosphorylation (Giet *et al.*, 2002; Barnard *et al.*, 2005; Kinoshita *et al.*, 2005), an important question for the future is how TACC3 may function to integrate signaling cascades downstream of axon guidance cue signals in order to control MT dynamics in growth cones, as well as in other cell types.

MATERIALS AND METHODS

Embryos

Eggs obtained from female *X. laevis* frogs (NASCO, Fort Atkinson, WI) were fertilized in vitro, dejellied, and cultured at 13–22°C in 0.1X Marc's modified Ringer's (MMR) using standard methods (Sive *et al.*, 2010). Embryos were staged according to Nieuwkoop and Faber (1994). All experiments were approved by the Boston College Institutional Animal Care and Use Committee and were performed according to national regulatory standards.

Culture of *Xenopus* embryonic explants

Embryos were cultured in 0.1× MMR at 22°C to stages 22–24, and each neural tube was dissected into approximately 20 similarly sized explants (Tanaka and Kirschner, 1991; Lowery *et al.*, 2013). The neural tube explants were plated in culture medium on poly-L-lysine (100 µg/ml)– and laminin (20 µg/ml)-coated coverslips attached to a plastic culture dish with a hole drilled in the center (imaging chambers described in Gomez *et al.*, 2003). Outgrowing axons and neural crest cells were imaged at room temperature 18–24 h after plating. For imaging of nonneural cells, somite tissue flanking the neural tube was dissected and plated on poly-L-lysine (100 µg/ml)– and fibronectin (100 µg/ml)-coated coverslips.

Constructs and RNA

Capped mRNA was transcribed in vitro using SP6 or T7 mMessage mMachine Kit (Life Technologies, Grand Island, NY). RNA was purified with LiCl precipitation and resuspended in nuclease-free water. Constructs used were GFP-TACC3 (TACC3 pET30a was gift from the Richter lab, University of Massachusetts Medical School, Worcester, MA), GFP-TACC3-NdeI, GFP-TACC3-CC2del, GFP-TACC3-CC1/2 (see Figure 5A for amino acid residues for each deletion construct, based on GenBank accession number NP_001081964.1), TACC3-GFP, mKate2-TACC3 (all TACC3 constructs subcloned into pCS2+

vector), mKate2-tubulin (Shcherbo *et al.*, 2009) in pT7TS, EB1-GFP in pCS107 (a gift from the Danilchik lab, Oregon Health Sciences University, Portland, OR), mKate2-EB1 in pCS2+, and XMAP215-GFP (a gift from the Hyman lab, Max Planck Institute of Molecular Cell Biology and Genetics, Dresden, Germany; Widlund *et al.*, 2011) subcloned into pT7TS. The dorsal blastomeres of embryos were injected four times at the two- to four-cell stage (in 0.1× MMR containing 5% Ficoll) with the following total mRNA amount per embryo: 100–300 pg of EB1-GFP or mKate2-EB1, 3000 pg of XMAP215-GFP, 900 pg of mKate2-tubulin, and 1000 pg of GFP-TACC3, mKate2-TACC3, or TACC3-mEmerald.

Morpholinos

MOs targeted to the translation start site of *X. laevis* TACC3 (5′-AGTTGTAGGCTCATTCTAAACAGGA-3′), start site of XMAP215 (Lowery *et al.*, 2013), or standard control MO (5′-cctcttacctcagttacaatttata-3′; purchased from Gene Tools [Philomath, OR]) were injected into two- to four-cell-stage embryos (50–80 ng/embryo for TACC3 and control MOs, 6–8 ng/embryo for XMAP215 MO). Protein knockdown was assessed by Western blot of embryos at stages 35–36. In rescue experiments, MO was injected along with mRNA in the same injection solution.

Western blotting and immunoprecipitation

Embryos were lysed in buffer (50 mM Tris, pH 7.5, 5% glycerol, 0.2% Igepal, 1.5 mM $MgCl_2$, 125 mM NaCl, 25 mM NaF, 1 mM Na_3VO_4, 1 mM dithiothreitol, supplemented with Complete Protease Inhibitor cocktail with or without EDTA [Roche, Indianapolis, IN]). For collection of neural/axonal lysates, neural tube explants were grown on coverslips overnight. Medium was then removed and replaced with lysis buffer (as described), and cultures were scraped to obtain the neural tissue. Blotting was carried out using goat anti–*X. laevis* TACC3 (1:500; sc-27046; Santa Cruz Biotechnology, Dallas, TX) and rabbit anti-XMAP215 (1:2500; a gift from the Hyman lab). Mouse anti–β-actin (1:2500; ab8224; Abcam) was used as a loading control. For TACC3 detection, 1% immunoglobulin G (IgG)-free bovine serum albumin (BSA) in phosphate-buffered saline/Tween-20 (PBST) was used to block nitrocellulose membrane. For other antibodies, 2% nonfat milk was used. Detection was done by chemiluminescence using Amersham ECL Western Blot reagent (GE Healthcare, Pittsburgh, PA). The bands were quantified by densitometry using Photoshop (Adobe, San Jose, CA), and the data and graphs were compiled in Excel (Microsoft, Redmond, WA).

Immunocytochemistry

Embryonic explant cultures were fixed in 100% cold methanol for 3 min and then rinsed in PBST and blocked in 0.1% Triton-X and 1% IgG-free BSA in PBS before antibody incubation. Immunostaining was carried out using goat anti-TACC3 (1:1000; sc-27046; Santa Cruz Biotechnology) and mouse anti-tubulin DM1α (1:1000; Sigma-Aldrich, St. Louis, MO). Donkey anti-goat Alexa Fluor 488 and donkey anti-mouse Alexa Fluor 568 antibodies (1:1000; Life Technologies) were used as secondary antibodies.

Confocal microscopy

Both live and fixed images were collected with a Yokogawa CSU-X1M 5000 spinning disk confocal on a Zeiss Axio Observer inverted motorized microscope with a Zeiss 63× Plan Apo 1.4 numerical aperture (NA) lens. Images were acquired with a Hamamatsu OCRA R2 charge-coupled device camera controlled with Zen software (Zeiss, Thornwood, NY). For time lapse, images were collected every 2 s for 1–3 min. Laser power for 488 nm was 30%, with exposure time 1000–1500 ms. Laser power of 561 nm was 25%, with exposure time 850–1500 ms. For imaging of immunostaining, laser power for 488 nm was set to 25%, with 95-ms exposure; for 561 nm, laser power was 12% with exposure time 800 ms. For two-color colocalizations in Figure 6, the TACC3 channel was translated in the *x*-axis, after calculating the frame-to-frame velocity of the growing MT plus end, in order to account for the 1-s time delay between channels, for each examined MT (using the Translate function of ImageJ [National Institutes of Health, Bethesda, MD]). To further confirm correct translation, time-lapse colocalizations were examined with both combinations of imaging—red channel first, green channel second; then green channel first, red channel second.

Axon outgrowth imaging

For axon outgrowth analysis, images were collected on a Zeiss Axio Observer inverted motorized microscope with a Zeiss 20× N-Achroplan 0.45 NA phase contrast lens, using a Zeiss AxioCam camera controlled with Zen software. Images were compiled and analyzed for axon outgrowth parameters (numbers of axons per explant and length of axons) using ImageJ.

PlusTipTracker software analysis

MT dynamics was analyzed from EB1-GFP or mKate2-EB1 movies using plusTipTracker (Applegate *et al.*, 2011; Lowery *et al.*, 2013; Stout *et al.*, 2014). We previously validated the imaging conditions and tracking parameters used in this study for accurate detection of EB1 comets in *X. laevis* growth cones (Stout *et al.*, 2014). The same parameters were used for all movies: maximum gap length, eight frames; minimum track length, three frames; search radius range, 5–12 pixels; maximum forward angle, 50°, maximum backward angle, 10°; maximum shrinkage factor, 0.8; fluctuation radius, 2.5 pixels; time interval, 2 s. Only growth cones with a minimum number of 10 MT tracks in a 1-min time lapse were included for analysis. The Peltier Tech Box and Whisker Chart Utility for Excel was used to make box plots. Because MT dynamics parameters were compiled from multiple individual experiments, and there can be significant day-to-day fluctuations in control MT dynamics (in part, based on room temperature fluctuations), the final compiled data were normalized relative to the mean of the control data for each experiment.

Image analysis and statistics

Phenotypic quantification was typically performed blind of genotype and from multiple experiments to ensure reproducibility. Fluorescently tagged TACC3 and XMAP215 MT plus end accumulations were measured with the Line tool in ImageJ along their longest axis, which was defined from their trajectory in the previous and subsequent frames. Line intensities were gathered using Plot Profile, and puncta lengths were determined where fluorescence signal became visually and statistically higher than noise. Cytoplasmic measurements were also obtained and used to normalize for overall expression level of each construct. Graphs were made in Excel, and histograms were generated using the Analysis Tool Pak. To determine statistical differences for axon and MT parameters, unpaired two-tailed *t* tests were used for comparing two conditions, whereas analysis of variance tests were used to compare multiple conditions (GraphPad, La Jolla, CA). For determining statistical differences for Western blot densitometry, since the distributions were not normal, a Kruskal–Wallis test was used (www.XLSTAT.com).

ACKNOWLEDGMENTS

We thank members of the Lowery lab for helpful discussions. We thank Gary Brouhard, David Burgess, Erik Folker, Elizabeth McNeill,

and Abigail Antoine for helpful critiques of the manuscript. We also thank Charles Baker, Salvatore D'Amico, Christopher Lucaj, Jonathan Boudreau, Taylor Nagel, and Xiaolin Chen for technical assistance with experiments and Nancy McGilloway and Todd Gaines for excellent *Xenopus* husbandry. We are grateful to Bret Judson of the Boston College Microscopy Suite for use of the phase objective; Doug Fishkind and John Wailes of Zeiss for image acquisition assistance; and the National *Xenopus* Resource for training in *Xenopus* imaging. L.A.L. is funded by National Institutes of Health R00 MH095768, and E.A.B. is funded by a National Science Foundation predoctoral fellowship.

REFERENCES

Akhmanova A, Steinmetz MO (2008). Tracking the ends: a dynamic protein network controls the fate of microtubule tips. Nat Rev Mol Cell Biol 9, 309–322.

Applegate KT, Besson S, Matov A, Bagonis MH, Jaqaman K, Danuser G (2011). plusTipTracker: quantitative image analysis software for the measurement of microtubule dynamics. J Struct Biol 176, 168–184.

Barnard DC, Cao Q, Richter JD (2005). Differential phosphorylation controls Maskin association with eukaryotic translation initiation factor 4E and localization on the mitotic apparatus. Mol Cell Biol 25, 7605–7615.

Bellanger JM, Gonczy P (2003). TAC-1 and ZYG-9 form a complex that promotes microtubule assembly in C. elegans embryos. Curr Biol 13, 1488–1498.

Brouhard GJ, Stear JH, Noetzel TL, Al-Bassam J, Kinoshita K, Harrison SC, Howard J, Hyman AA (2008). XMAP215 is a processive microtubule polymerase. Cell 132, 79–88.

Cullen CF, Ohkura H (2001). Msps protein is localized to acentrosomal poles to ensure bipolarity of Drosophila meiotic spindles. Nat Cell Biol 3, 637–642.

Engel U, Zhan Y, Long JB, Boyle SN, Ballif BA, Dorey K, Gygi SP, Koleske AJ, Vanvactor D (2014). Abelson phosphorylation of CLASP2 modulates its association with microtubules and actin. Cytoskeleton (Hoboken) 71, 195–209.

Gergely F, Karlsson C, Still I, Cowell J, Kilmartin J, Raff JW (2000a). The TACC domain identifies a family of centrosomal proteins that can interact with microtubules. Proc Natl Acad Sci USA 97, 14352–14357.

Gergely F, Kidd D, Jeffers K, Wakefield JG, Raff JW (2000b). D-TACC: a novel centrosomal protein required for normal spindle function in the early Drosophila embryo. EMBO J 19, 241–252.

Giet R, McLean D, Descamps S, Lee MJ, Raff JW, Prigent C, Glover DM (2002). Drosophila Aurora A kinase is required to localize D-TACC to centrosomes and to regulate astral microtubules. J Cell Biol 156, 437–451.

Gomez TM, Harrigan D, Henley J, Robles E (2003). Working with Xenopus spinal neurons in live cell culture. Methods Cell Biol 71, 129–156.

Groisman I, Huang YS, Mendez R, Cao Q, Theurkauf W, Richter JD (2000). CPEB, maskin, and cyclin B1 mRNA at the mitotic apparatus: implications for local translational control of cell division. Cell 103, 435–447.

Honnappa S, Gouveia SM, Weisbrich A, Damberger FF, Bhavesh NS, Jawhari H, Grigoriev I, van Rijssel FJ, Buey RM, Lawera A, *et al.* (2009). An EB1-binding motif acts as a microtubule tip localization signal. Cell 138, 366–376.

Hur EM, Saijilafu, Lee BD, Kim SJ, Xu WL, Zhou FQ (2011). GSK3 controls axon growth via CLASP-mediated regulation of growth cone microtubules. Genes Dev 25, 1968–1981.

Kinoshita K, Noetzel TL, Pelletier L, Mechtler K, Drechsel DN, Schwager A, Lee M, Raff JW, Hyman AA (2005). Aurora A phosphorylation of TACC3/maskin is required for centrosome-dependent microtubule assembly in mitosis. J Cell Biol 170, 1047–1055.

Le Bot N, Tsai MC, Andrews RK, Ahringer J (2003). TAC-1, a regulator of microtubule length in the C. elegans embryo. Curr Biol 13, 1499–1505.

Lee H, Engel U, Rusch J, Scherrer S, Sheard K, Van Vactor D (2004). The microtubule plus end tracking protein Orbit/MAST/CLASP acts downstream of the tyrosine kinase Abl in mediating axon guidance. Neuron 42, 913–926.

Lee MJ, Gergely F, Jeffers K, Peak-Chew SY, Raff JW (2001). Msps/XMAP215 interacts with the centrosomal protein D-TACC to regulate microtubule behaviour. Nat Cell Biol 3, 643–649.

Li W, Miki T, Watanabe T, Kakeno M, Sugiyama I, Kaibuchi K, Goshima G (2011). EB1 promotes microtubule dynamics by recruiting Sentin in Drosophila cells. J Cell Biol 193, 973–983.

Long JB, Bagonis M, Lowery LA, Lee H, Danuser G, Van Vactor D (2013). Multiparametric analysis of CLASP-interacting protein functions during interphase microtubule dynamics. Mol Cell Biol 33, 1528–1545.

Lowery LA, Stout A, Faris AE, Ding L, Baird MA, Davidson MW, Danuser G, Van Vactor D (2013). Growth cone-specific functions of XMAP215 in restricting microtubule dynamics and promoting axonal outgrowth. Neural Dev 8, 22.

Lowery LA, Van Vactor D (2009). The trip of the tip: understanding the growth cone machinery. Nat Rev Mol Cell Biol 10, 332–343.

Marx A, Godinez WJ, Tsimashchuk V, Bankhead P, Rohr K, Engel U (2013). Xenopus cytoplasmic linker-associated protein 1 (XCLASP1) promotes axon elongation and advance of pioneer microtubules. Mol Biol Cell 24, 1544–1558.

Maurer SP, Cade NI, Bohner G, Gustafsson N, Boutant E, Surrey T (2014). EB1 accelerates two conformational transitions important for microtubule maturation and dynamics. Curr Biol 24, 372–384.

Nakamura S, Grigoriev I, Nogi T, Hamaji T, Cassimeris L, Mimori-Kiyosue Y (2012). Dissecting the nanoscale distributions and functions of microtubule-end-binding proteins EB1 and ch-TOG in interphase HeLa cells. PloS One 7, e51442.

Neukirchen D, Bradke F (2011). Cytoplasmic linker proteins regulate neuronal polarization through microtubule and growth cone dynamics. J Neurosci 31, 1528–1538.

Nieuwkoop PD, Faber J (1994). Normal Table of Xenopus Laevis (Daudin), New York: Garland.

O'Brien LL, Albee AJ, Liu L, Tao W, Dobrzyn P, Lizarraga SB, Wiese C (2005). The Xenopus TACC homologue, maskin, functions in mitotic spindle assembly. Mol Biol Cell 16, 2836–2847.

Peset I, Seiler J, Sardon T, Bejarano LA, Rybina S, Vernos I (2005). Function and regulation of Maskin, a TACC family protein, in microtubule growth during mitosis. J Cell Biol 170, 1057–1066.

Peset I, Vernos I (2008). The TACC proteins: TACC-ling microtubule dynamics and centrosome function. Trends Cell Biol 18, 379–388.

Rochlin MW, Wickline KM, Bridgman PC (1996). Microtubule stability decreases axon elongation but not axoplasm production. J Neurosci 16, 3236–3246.

Sadek CM, Pelto-Huikko M, Tujague M, Steffensen KR, Wennerholm M, Gustafsson JA (2003). TACC3 expression is tightly regulated during early differentiation. Gene Expr Patterns 3, 203–211.

Samereier M, Baumann O, Meyer I, Graf R (2011). Analysis of Dictyostelium TACC reveals differential interactions with CP224 and unusual dynamics of Dictyostelium microtubules. Cell Mol Life Sci 68, 275–287.

Shcherbo D, Murphy CS, Ermakova GV, Solovieva EA, Chepurnykh TV, Shcheglov AS, Verkhusha VV, Pletnev VZ, Hazelwood KL, Roche PM, *et al.* (2009). Far-red fluorescent tags for protein imaging in living tissues. Biochem J 418, 567–574.

Sive HL, Grainger RM, Harland RM (2010). Microinjection of Xenopus embryos. Cold Spring Harbor Protocols 2010, pdb.ip81.

Srayko M, Quintin S, Schwager A, Hyman AA (2003). Caenorhabditis elegans TAC-1 and ZYG-9 form a complex that is essential for long astral and spindle microtubules. Curr Biol 13, 1506–1511.

Stebbins-Boaz B, Cao Q, de Moor CH, Mendez R, Richter JD (1999). Maskin is a CPEB-associated factor that transiently interacts with eIF-4E. Mol Cell 4, 1017–1027.

Stepanova T, Slemmer J, Hoogenraad CC, Lansbergen G, Dortland B, De Zeeuw CI, Grosveld F, van Cappellen G, Akhmanova A, Galjart N (2003). Visualization of microtubule growth in cultured neurons via the use of EB3-GFP (end-binding protein 3-green fluorescent protein). J Neurosci 23, 2655–2664.

Stout A, D'Amico S, Enzenbacher T, Ebbert P, Lowery LA (2014). Using plusTipTracker software to measure microtubule dynamics in Xenopus laevis growth cones. J Vis Exp, e52138.

Tanaka E, Ho T, Kirschner MW (1995). The role of microtubule dynamics in growth cone motility and axonal growth. J Cell Biol 128, 139–155.

Tanaka EM, Kirschner MW (1991). Microtubule behavior in the growth cones of living neurons during axon elongation. J Cell Biol 115, 345–363.

Tessmar K, Loosli F, Wittbrodt J (2002). A screen for co-factors of Six3. Mech Dev 117, 103–113.

Thakur HC, Singh M, Nagel-Steger L, Kremer J, Prumbaum D, Fansa EK, Ezzahoini H, Nouri K, Gremer L, Abts A, *et al.* (2014). The centrosomal adaptor TACC3 and the microtubule polymerase chTOG interact via defined C-terminal subdomains in an Aurora-A kinase-independent manner. J Biol Chem 289, 74–88.

van der Vaart B, Franker MA, Kuijpers M, Hua S, Bouchet BP, Jiang K, Grigoriev I, Hoogenraad CC, Akhmanova A (2012). Microtubule plus-end

tracking proteins SLAIN1/2 and ch-TOG promote axonal development. J Neurosci 32, 14722–14728.
van der Vaart B, Manatschal C, Grigoriev I, Olieric V, Gouveia SM, Bjelic S, Demmers J, Vorobjev I, Hoogenraad CC, Steinmetz MO, *et al.* (2011). SLAIN2 links microtubule plus end-tracking proteins and controls microtubule growth in interphase. J Cell Biol 193, 1083–1099.
Widlund PO, Stear JH, Pozniakovsky A, Zanic M, Reber S, Brouhard GJ, Hyman AA, Howard J (2011). XMAP215 polymerase activity is built by combining multiple tubulin-binding TOG domains and a basic lattice-binding region. Proc Natl Acad Sci USA 108, 2741–2746.
Xie Z, Moy LY, Sanada K, Zhou Y, Buchman JJ, Tsai LH (2007). Cep120 and TACCs control interkinetic nuclear migration and the neural progenitor pool. Neuron 56, 79–93.
Yang YT, Wang CL, Van Aelst L (2012). DOCK7 interacts with TACC3 to regulate interkinetic nuclear migration and cortical neurogenesis. Nat Neurosci 15, 1201–1210.
Zhou FQ, Zhou J, Dedhar S, Wu YH, Snider WD (2004). NGF-induced axon growth is mediated by localized inactivation of GSK-3beta and functions of the microtubule plus end binding protein APC. Neuron 42, 897–912.